Bilayer charge asymmetry destabilizes membranes upon poration

Fernanda S. C. Leomil[1,2,†], *Mareike Stephan*[2,†], *Karin A. Riske*[1,*], *Rumiana Dimova*[2,*]

[1] Departamento de Biofísica, Universidade Federal de São Paulo, São Paulo 04039-032, Brazil
[2] Max Planck Institute of Colloids and Interfaces, 14776 Potsdam, Germany
[†] Authors with equal contribution
[*] Correspondence: Rumiana.Dimova@mpikg.mpg.de and kariske@unifesp.br

Key words: NBD Quenching assay, electroporation, membrane charge asymmetry, pore edge tension, GUV

Abstract

Membrane asymmetry is ubiquitous in cell membranes particularly with respect to lipids, whereby charged lipids are mainly restricted to the inner monolayer. We investigate the influence of anionic lipid asymmetry on the stability of giant unilamellar vesicles (GUVs), minimal plasma membrane models. To quantify asymmetry, we apply a fluorescence quenching assay, which is often difficult to reproduce and caution in handling the quencher is generally underestimated. Thus, we first optimize this assay and then apply it to GUVs prepared with the inverted emulsion transfer protocol using increasing fractions of anionic lipids restricted to one leaflet. This protocol is found to produce highly asymmetric bilayers, but with ~20% interleaflet mixing. To probe the stability of asymmetric *vs* symmetric membranes, we expose the GUVs to porating DC pulses and monitor the fraction of destabilized vesicles. The pulses open macropores, and the GUVs either completely recover their integrity or become destabilized exhibiting leakage or bursting/collapse. Destabilization is much more pronounced in asymmetrically charged membranes, which is corroborated by pore edge tension data showing considerable decrease with asymmetry. Rendering GUV membrane asymmetric from exposure to different transmembrane pH, we confirm that poration-triggered destabilization does not depend on the approach used to generate membrane asymmetry.

1   Introduction

A typical eukaryotic cell membrane is highly asymmetric in the distribution of its main constituents, which is essential to ensure the distinct functions of cells. The asymmetry is comprehensive in respect to membrane proteins and carbohydrates: integral proteins exhibit always the same orientation, peripheral proteins are only found associated with one of the leaflets and carbohydrates attached to proteins and lipids only face the external medium, where they are crucial to cell signaling. Importantly, the lipid bilayer composition is also highly asymmetric [1]. Specifically in mammalian membranes, phosphatidylcholine and sphingomyelin are found in abundance in the outer monolayer, while phosphatidylethanolamine and anionic lipids, such as phosphatidylserine and phosphatidylinositol, are most commonly found in the inner leaflet, giving rise to a charge asymmetry across the membrane [2,3]. Lipid asymmetry affects many membrane properties, such as curvature, shape, permeability and stability of cell membranes. The loss of this asymmetry implies crucial physiological consequences [4–7], as for instance the apoptotic

1

cascade followed by the externalization of phosphatidylserine [8,9]. Therefore, healthy cells dedicate substantial effort and energy to sustain membrane asymmetry. This is achieved mainly by the work of flippases and floppases, which are enzymes that transport lipids from one leaflet to the other in order to keep the desired lipid asymmetry [10,11], but also via protein-free processes [12] (more relevant for model membranes). Reversible lipid asymmetry is now also being recognized as a factor influencing intracellular signaling and intercellular communication [13]. These efforts highlight the importance of asymmetry and merit in being thoroughly investigated.

Membrane stability is of essential importance to cell viability, as the first collective property of the plasma membrane is to act as a boundary to the cell, regulating the traffic of substances. The integrity of the cell membrane relies mainly on the material properties of the constituting lipid bilayer, which due to the hydrophobic effect forms a cohesive and robust film that is nonetheless soft and able to bend. These properties are sensitive to the lipid composition and are affected by the asymmetric distribution of lipids [1], an effect that can be further enhanced when charge asymmetry is present. Even though membranes are stable, they can rupture through the opening of a pore, for example in response to mechanical stress. Poration can lead to cell death in the case that a quick resealing of the pore fails [14,15]. Pores in cell membranes can also be created on purpose, with the application of a high-intensity electric pulse [16], as in clinical procedures, favoring the entrance of different molecules into cells for which the membrane is generally impermeable [17]. Due to its efficiency, this method (named electroporation or electropermeabilization) has become a common approach in the treatment of various types of cancer [18–22]. Additionally, it is being used for gene therapy [23,24] and to encapsulate or promote cargo release in drug delivery systems [25].

Model membranes have emerged as a useful tool to allow a better understanding of physiological phenomena involving cell membranes. Being composed of a minimal set of components, they represent a simplified version of complex biomembranes and are less susceptible to possible interferences from different processes. They also offer the benefit of allowing independent changes of a single parameter at a time. In particular, giant unilamellar vesicles (GUVs) [26] stand out as an ideal system since they replicate the plasma membrane in terms of size (10 - 100 µm) and curvature and are large enough to be observed and manipulated under an optical microscope. GUVs internal and external aqueous solutions are often chosen to be sucrose and glucose, respectively. In these settings, when observed under phase contrast microscopy, the refractive indices of the two sugar solutions create a contrast across the vesicle membrane making the GUVs interface appear as dark contour with a bright halo around. Furthermore, any discontinuity in the membrane (such as the one caused by the opening of a micron-sized pore) can be easily visualized [27]. The response of GUVs to electric pulses has been studied in detail, revealing interesting relaxation properties of lipid bilayers [27,28], including pore opening and closing dynamics [29–31]. It was shown that while electric pulses applied to zwitterionic GUVs composed of POPC (palmitoyl oleoyl phosphatidylcholine) caused the opening of transient macropores that lasted about 50 ms, GUVs containing the anionic lipid POPG (palmitoyl oleoyl phosphatidylglycerol) could be completely disrupted and collapse after the pulse [32]. The presence of POPG and other anionic lipids and molecules was shown to render the membrane more susceptible to the electric pulses, giving rise to leaky membranes or to complete vesicle collapse (bursting) [33–35]. A fundamental membrane material property that characterizes the stability of pores formed in a membrane is the pore edge tension (γ), which reflects the energy cost of maintaining an open pore in the membrane [36], and is crucial for plasma membrane repair processes. If the cost to rearrange the lipids in the pore rim is too low, as in the case of unstable membranes, the vesicle will burst due to continuous opening of the pore, associated with low edge tension values. The pore edge tension

2

can be measured from the dynamics of macropore closure [29,34,36]. Earlier data have shown a two-fold reduction for membranes containing 50 mol% charged lipids [32–34] compared to neutral membranes. Interestingly, the increased destabilization was not observed to depend on the specific anionic lipid, but rather on the surface charge density in the membrane [42].

The above-mentioned previous studies were performed with symmetric lipid bilayers of giant vesicles prepared mainly by the conventional electroformation method [37]. Lately, several methods have been developed to allow for the preparation of asymmetric membranes to mimic cell membrane asymmetry. Some of them are based on cyclodextrin-mediated lipid exchange [38–40], others (and more abundantly applied to the preparation of GUVs) are based on the phase-transfer method (also known as droplet-transfer or emulsion transfer) [41–44]. However, it is of utmost importance to validate the preparation method by probing the actual membrane asymmetry of the generated vesicles. Different methodologies have been reported so far, including nuclear magnetic resonance (NMR) analysis [45–48], neutron reflectometry [49], small-angle neutron scattering [50] and copper-free click chemistry between outer leaflet lipids and fluorophores [51]. Monitoring the formation of inward or outward nanotubes upon vesicle deflation also offers a way to infer the presence of asymmetry [52–55]. While NMR and click chemistry-based techniques are not feasible in every laboratory setup and/or cannot be applied to giant vesicles, spontaneous tubulation offers an easy and straightforward visualization. However, this is not a very quantitative approach as tubulation in vesicles is not amenable to precise characterization and can vary from vesicle to vesicle because of the different area-to-volume values. An alternative technique is the fluorescence quenching assay, first described in 1991 by McIntyre and Sleight as an assay to determine asymmetric fluorophore distributions in small unilamellar vesicles (SUVs) [56]. Since this first report, the quenching assay has been ubiquitously applied to access membrane asymmetry in small, large and giant unilamellar vesicles or even in living cells, see e.g. [53,56–59]. The assay is based on the reduction of NBD (nitrobenzoxadiazol)-labeled lipids by dithionite ions, causing an irreversible inactivation (quenching) of the fluorophore, Figure 1A. Verbal exchange with researchers in other groups has suggested that this assay is not easy to reproduce from lab to lab and between users. This is why, here, we thoroughly explored and identified conditions that must be ensured for a functional and reproducible quenching assay.

Using the optimized assay, we investigate the influence of charge asymmetry in GUVs subjected to electroporation. Asymmetric GUVs composed of POPC with increasing molar fractions of POPG restricted to one of the leaflets are prepared using the inverted emulsion technique. The success of the preparation method and the degree of asymmetry achieved is verified using the quenching of NBD-labeled PG lipid by sodium dithionite. We then interrogate the stability of asymmetric GUVs compared to symmetric ones, by quantifying the fraction of destabilized vesicles upon electroporation and by measuring the pore edge tension, which governs pore closure. We show that membrane destabilization can be much more pronounced if charge asymmetry, as in the case of real cells, is present. Moreover, we raise concerns about possible oil contamination in the membranes of GUVs prepared via the inverted emulsion technique. Finally, an alternative preparation method of asymmetric GUVs, based on pH asymmetry, is put forward to demonstrate that charge asymmetry is the main source of membrane destabilization.
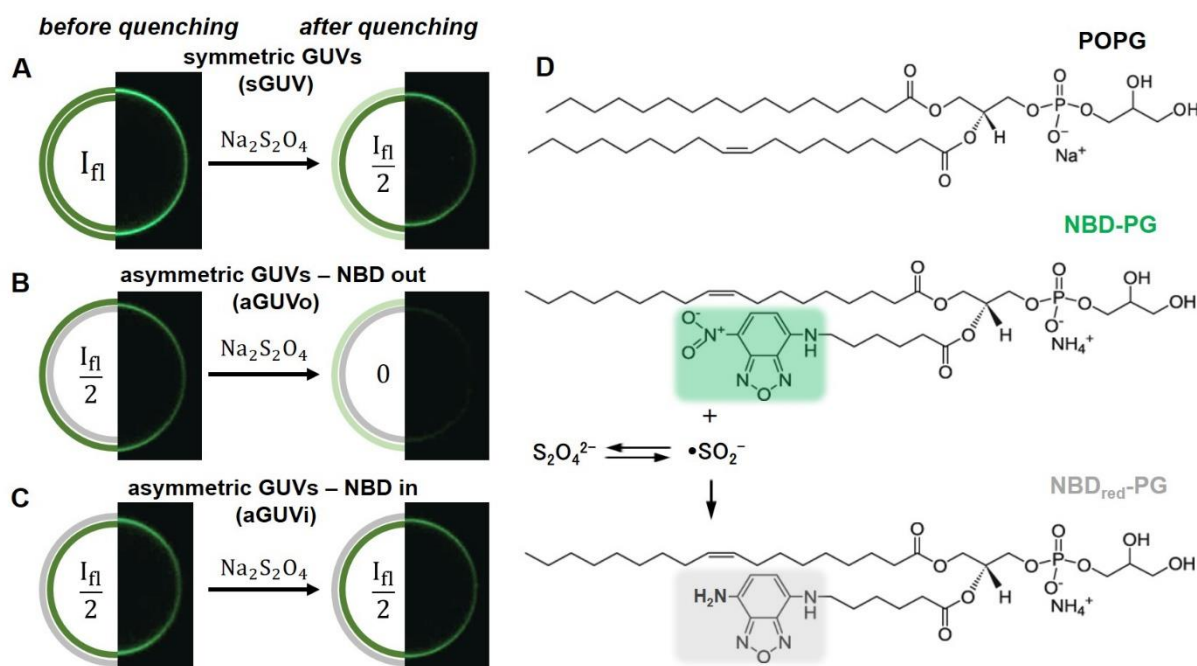
Figure 1. Principle of the quenching assay for evaluating membrane asymmetry in GUVs and chemical structures of molecules. (A-C) The cartoons and example confocal cross sections of GUV halves illustrate how the vesicle fluorescence intensity, I_{fl}, should change upon external addition of sodium dithionite when the distribution of the quenched fluorophore in the initial GUV is (A) symmetric (sGUVs) or (B, C) asymmetric with the fluorescent lipid located at the outer or inner leaflet (aGUVo or aGUVi respectively). The vesicles in the shown confocal cross sections had diameters between 20 and 40 μm. (D) Chemical structures of the anionic lipid POPG, its fluorescence analogue NBD-PG and the effect of sodium dithionite on the fluorescent group. In solution, the dithionite ion $S_2O_4^{2-}$ is in equilibrium with the $\bullet SO_2^-$ radical, which reduces the nitro group of NBD to its corresponding amine. The reduced NBD-PG (NBD$_{red}$-PG) is non-fluorescent.

2. Results and Discussion

Asymmetric GUVs made of POPC and increasing fractions of POPG restricted to one of the leaflets were prepared by the inverted emulsion protocol [43]. The efficiency of the method in generating asymmetric GUVs was quantified using the assay based on NBD quenching by sodium dithionite. In the following, we first describe the principle of the method and its application to symmetric and asymmetric vesicles (Figure 1). Next, the method is optimized, which is crucial for valid probing of the degree of asymmetry of the obtained GUVs. Then, the stability of asymmetric GUVs was assessed by the application of DC pulses and quantification of destabilization effects and pore edge tension. Finally, the asymmetry in the vesicle bilayer was achieved by exposing the GUV membrane to different pH conditions inside and outside. These findings aimed at demonstrating that membrane destabilization is caused by charge asymmetry and not by the inverted emulsion protocol, which can result in traces of residual oil in the membrane.

2.1. Principle of the quenching assay

The quenching assay is based on the irreversible reduction of the nitro group of the fluorescent probe NBD by the radical $\bullet SO_2^-$ (in equilibrium with the dithionite ion $S_2O_4^{2-}$) to its corresponding amine, which is non-fluorescent [56], see Figure 1D. The fluorescence signal can be quantitatively assessed from confocal microscopy cross sections of GUVs (Figure 1A-C), see also sections 4.4 and 4.5 for details on the image acquisition and processing. For the

4

optimization of the quenching protocol, POPC GUVs with a symmetric distribution of 1 mol% NBD-PG (a PG lipid labeled with NBD in one of the hydrophobic tails, see Figure 1D) were prepared by the conventional electroformation method. Due to the structural and charge similarities, it is expected that NBD-PG distributes across the membrane in a similar manner as POPG and can be treated as its fluorescent representative. Since the NBD group has a relatively high polarity, it is assumed that the lipid tail kinks allowing sodium dithionite to access the NBD fluorophore. Because the membrane is ideally impermeable to sodium dithionite, quenching is expected to only affect fluorophores exposed at the outer membrane leaflet. Therefore, a reduction of 50% in the fluorescence intensity of the membrane is expected due to the symmetric fluorophore distribution, see Figure 1A. For asymmetric vesicles with NBD-PG located only on the outer leaflet (aGUVo), the fluorescence signal should be completely quenched (Figure 1B), while for vesicles with NBD-PG located on the inner leaflet (aGUVi), no change is expected (Figure 1C). The assay requires precaution, since sodium dithionite is a strong reducing agent and unstable in aqueous solutions [60]. Depending on concentration, pH and oxygen access, dithionite shows different reactions [61]. Consequently, the optimization of substance handling and reaction conditions are crucial.

2.2. Optimization of the quenching assay

The first concern is to define the best conditions for the preparation of sodium dithionite stock solution. In aqueous environment and in aerobic conditions, sodium dithionite ($Na_2S_2O_4$) is oxidized to hydrogen sulphide ($NaHSO_3$) and hydrogen sulphate ($NaHSO_4$) causing a decrease of the solution pH [62], which then accelerates further dithionite auto-oxidation. Additional to increased acidity, high dithionite concentration accelerates the decomposition of the dithionite ion [60]. Therefore, the dithionite stock concentration was kept at maximum 0.1 M and not 1 M as described in other publications [53,56,59]. Highly concentrated 1 M sodium dithionite solutions showed yellow color and a strong sulfuric smell, indicating the formation of sulfur dioxide and sulfur. Stock solution concentrations lower than 0.1 M were also avoided to ensure that the volume of the dithionite solution added to the GUV sample is sufficient but small, preventing excessive vesicle dilution. The 0.1 M sodium dithionite solution was always freshly prepared and immediately used.

When the 0.1 M sodium dithionite stock solution was prepared in non-buffered 0.18 M glucose (neutral pH), which is the external solution of the GUVs, the pH of the solution dropped to 2. The addition of this non-buffered sodium dithionite solution to a GUV sample (final concentration 2.5 mM) resulted in permeabilized and defective GUVs and lipid aggregates (Figure 2A). Since alkaline pH-solutions stabilize the dithionite ion [56,60,61], we prepared the 0.1 M sodium dithionite stock solution in 1 M TrisHCl buffer at pH 10. Upon dilution into the working conditions, the GUV solution attained close to neutral pH. Quenching with buffered high pH stock solution is exemplified in Figure 2B. In the case when sodium dithionite was prepared in 1 M TrisHCl buffer pH 10, the GUVs maintained their integrity and only fluorophores at the outer leaflet were quenched (Figure 2B). The scatter in the data is a result of the different vesicles sizes (i.e. equatorial sections located higher above the chamber bottom and deeper in the sample) and inhomogeneous distribution of the dye across vesicles. Therefore, the data should be interpreted with precaution and quantitate comparison should be considered only from samples quenched at the same conditions. Note that the data in Figure 2B for the case of the non-buffered conditions (0.18 M glucose) is scarce because of the small number and defective GUVs surviving the treatment.
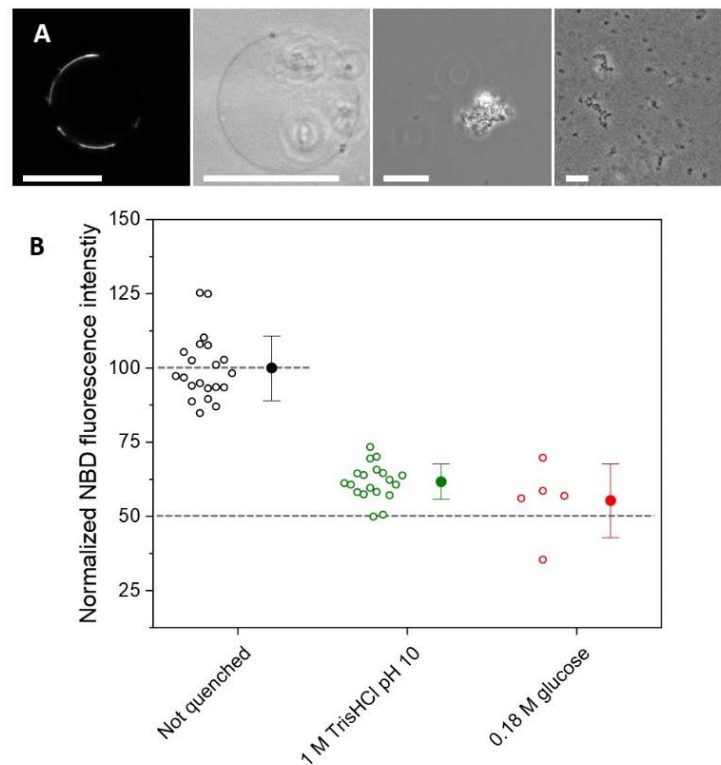
Figure 2: Non-buffered dithionite solutions affect GUV stability and do not allow for consistent quenching experiments. (A) Examples of GUVs and lipid aggregates observed when diluting POPC GUVs (1 mol % NBD-PG) with 0.1 M $Na_2S_2O_4$ prepared in 0.18 M glucose to a final concentration of 2.5 mM $Na_2S_2O_4$. The first image was acquired with confocal and the others with phase contrast microscopy. The scalebars correspond to 25 µm. (B) Normalized fluorescence intensities before quenching (black circles) and in the presence of 2.5 mM $Na_2S_2O_4$ added from stock solutions of 0.1 M dithionite prepared in 1 M TrisHCl pH 10 (green circles) or in 0.18 M glucose (red circles). Each open symbol represents measurements on one vesicle and mean values with standard deviation are shown on the right. The dashed lines are guides to the eye and indicate the original vesicles intensity (unquenched) and half of this initial mean value.

Other important parameters for the quenching assay are the working concentration of sodium dithionite and the incubation time. Note that different concentrations and incubation times have been implemented in the literature (most often using 10 mM final concentration prepared from 1M stock solutions, which, as indicated above, results in decomposition). Presumably, an additional adjustment of the dithionite concentration is required if very different total lipid concentrations are explored. Here, starting with the stock solution of 0.1 M $Na_2S_2O_4$ in 1 M TrisHCl pH 10 we tested different final working concentration (from 0.5 to 10 mM $Na_2S_2O_4$) and incubation times (from 1 to 15 minutes). The desired sodium dithionite concentration was added to the test tube containing the GUVs and after a specific incubation time, the suspension was further diluted 5-fold in order to decrease substantially the quencher concentration, reduce quenching rate, stop unwanted sample degradation and allow for observation and image acquisition (see Figure 3A that demonstrates the effect of quenching the fluorescence signal in both leaflets if the dilution step is not implemented). The results from exploring different incubation times (while implementing the 5-fold dilution step afterwards) are shown in Figure 3B,C. While incubation of 1 minute was not sufficient to inactivate all fluorophores at the outer leaflet, incubation for 5 minutes led to a quenching of roughly 50 % of the total fluorescence (Figure 3C). Longer incubation times of 10 and 15 minutes resulted in fluorescence reductions by more than 50 %, indicating transmembrane dithionite transfer and quenching of part of the inner leaflet fluorophores. Previous studies revealed that the outer leaflet was quenched in the first 50-70 seconds in the case of SUVs, which are much smaller

6

and highly curved [56]. Then, transfer of dithionite ions or radicals across the membrane was observed to occur at a slower rate leading to quenching of fluorophores residing in the inner leaflet as well (corroborating our results). The authors suggested that the membrane transfer of dithionite ions and radicals depends on the composition and structure of the observed membrane [56]. Therefore, in the following experiments, GUV samples were diluted to low dithionite concentrations 5 minutes after addition of the quenching agent.

Next, different dithionite concentrations in the final quenching sample were tested. Figure 3D shows that complete quenching of the outer leaflet of GUVs is observed already at final concentration of 2.5 mM. Using higher concentration (10 mM) resulted in fluorescence drops by more than 50 %, indicating that dithionite ions reached some of the inner leaflet fluorophores. We hypothesize that the presence of excess dithionite ions leads to the formation of more decomposition products, which destabilize the membrane and make it permeable for non-decomposed dithionite ions that can then quench the inner leaflet fluorophores. The minimum concentration needed to quench outer leaflet fluorophores depends on the number of fluorophores and on the number of GUVs present in the sample. Therefore, the optimal dithionite concentration for a particular sample should always be tested prior to the actual experiments. For our experimental conditions (roughly 10 µM final total lipid concentration), we chose to work with 2.5 mM dithionite and 5 min incubation time, which was sufficient to quench the NBD groups present only in the external leaflet without causing significant alterations in GUV integrity.
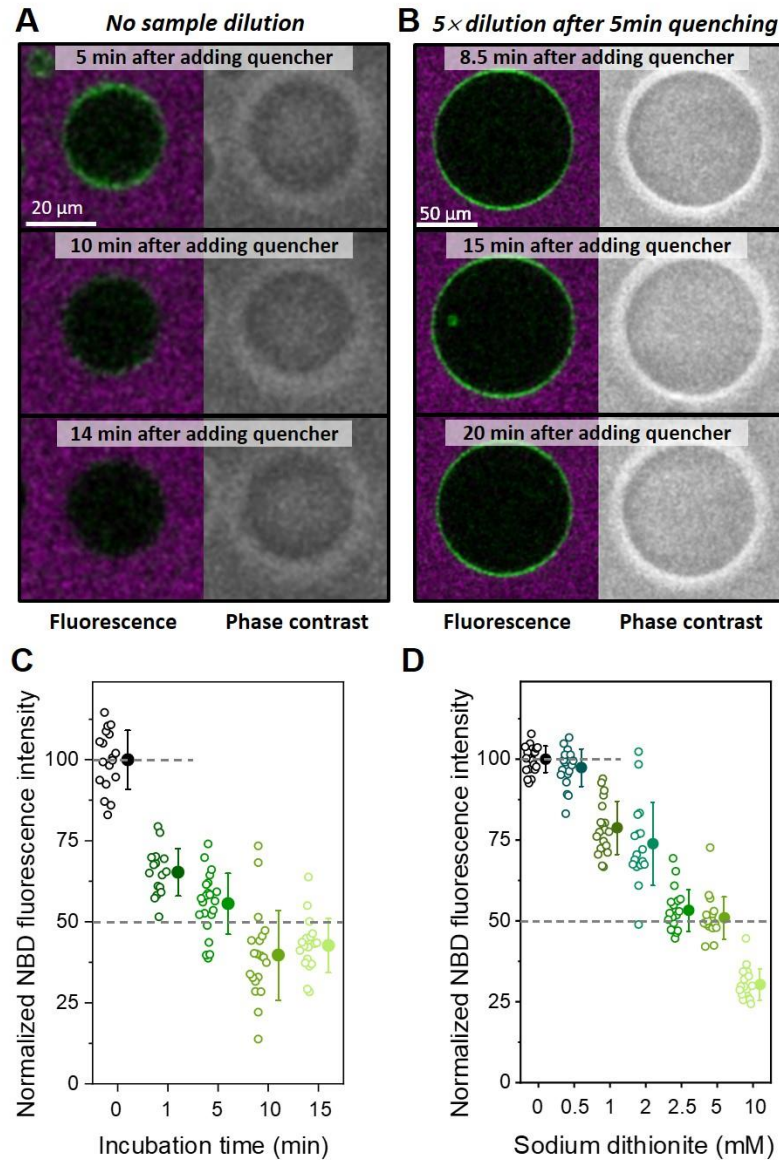
Figure 3: Effect of sample dilution, incubation time and sodium dithionite concentration on the quenching of the NBD fluorescence in GUVs. (A, B) Confocal and phase-contrast image sequences of two symmetric GUVs composed of POPC with 1 mol% NBD-PG (green) prepared with sucrose and then dispersed in glucose medium containing 10 μM of the water-soluble fluorescent dye Alexa 647 (purple). The quenching agent was added to a final concentration of 2.5 mM $Na_2S_2O_4$ and 5 min after incubation the sample was either directly transferred to the observation chamber (A) or 5-fold diluted in glucose and then transferred for observation (B). Both GUVs remain impermeable to the dye Alexa 647 and sucrose/glucose (optical contrast is maintained), but dithionite ions are able to quench NBD in both leaflets after 14 min in the absence of a dilution step (A). The dilution step restricts quenching to the outer leaflet only (B). (C) Normalized fluorescence intensities before (not quenched, indicated as 0 incubation time) and after quenching with 2.5 mM $Na_2S_2O_4$ for different incubation times followed by 5-fold dilution. (D) Normalized fluorescence intensities before (0) and after quenching of different sodium dithionite concentration for 5 minutes incubation time followed by 5-fold dilution. Each open symbol represents measurements on one vesicle and mean values with standard deviation are shown as solid symbols on the right. Typically, between 15 and 20 vesicles were measured per sample. The dashed lines are guides to the eye and indicate not-quenched and half of that mean value.

8

2.3. Membrane asymmetry of GUVs prepared via the inverted emulsion protocol

In the previous section, we determined important parameters to optimize the quenching assay for probing the membrane asymmetry. We then used the inverted emulsion protocol to obtain POPC GUVs containing 5 mol% POPG in total and 0.5 mol% NBD-PG. The PG lipids were distributed either symmetrically (referred to as sGUVs, with 5 mol% POPG in each membrane leaflet) or asymmetrically (aGUVs, with 10 mol% POPG in one of the leaflets). Two types of asymmetric GUVs were prepared: with POPG and NBD-PG restricted either to the inner (aGUVi) or outer (aGUVo) leaflet. Since we now have the control that sodium dithionite quenches about half of the NBD-PG dyes in sGUVs (Figure 3), we expect either full quenching when the NBD is present only in the outer layer (aGUVo) or no quenching at all if the NBD is restricted to the inner leaflet (aGUVi), as illustrated in Figure 1B,C. The normalized fluorescence intensity before and after quenching of sGUVs and aGUVs grown by the inverted emulsion protocol are shown in Figure 4. As expected, sGUVs have their fluorescence intensity decreased by 50% after addition of sodium dithionite, consistent with data for sGUVs produced via electroformation, thus demonstrating that the employed inverted emulsion protocol efficiently produces GUVs with symmetric distribution of the charged lipids. When aGUVi were exposed to the quenching agent, a signal reduction of ~25% was observed rather than the expected zero fluorescence intensity reduction. In the case of aGUVo, instead of a complete quenching of the fluorescence, residual fluorescence intensity was detected (~15%) after treatment with sodium dithionite. Since under the same experimental conditions the symmetric controls showed the expected reduction by 50%, and the integrity of the aGUVs was maintained (observed by preservation of optical contrast under phase contrast), the observed outcome indicates that the inverted emulsion protocol is not efficient in generating entirely asymmetric membranes. We conclude that some mixing (roughly about 20%) of the lipids originating from the different oil layers during the preparation procedure occurred, see estimates in Figure 4. Nonetheless, the inverted emulsion method ensured generation of membranes with a high degree of asymmetry.

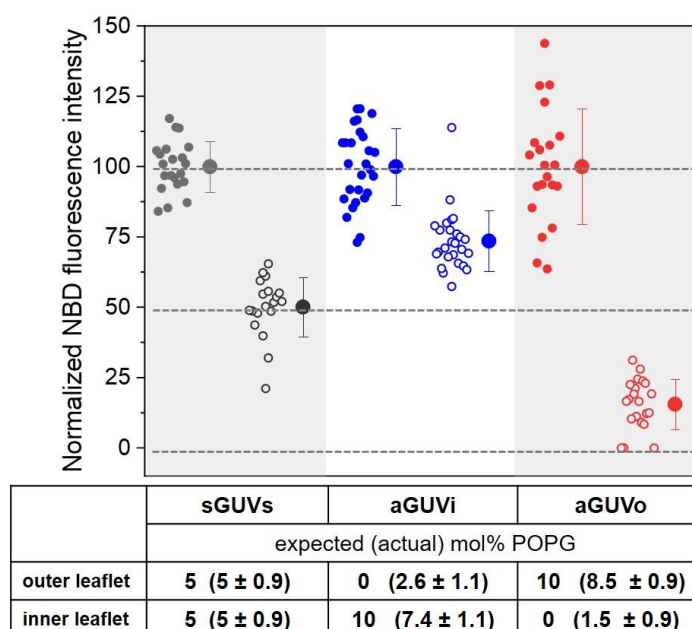|	sGUVs	aGUVi	aGUVo
	expected (actual) mol% POPG		
outer leaflet	5 (5 ± 0.9)	0 (2.6 ± 1.1)	10 (8.5 ± 0.9)
inner leaflet	5 (5 ± 0.9)	10 (7.4 ± 1.1)	0 (1.5 ± 0.9)

Figure 4: Normalized fluorescence intensities before (solid circles) and after (open circles) quenching of NBD-PG (0.5 mol%) for GUVs containing 5 mol% POPG symmetrically and asymmetrically distributed. Each data point represents measurements on one vesicle and solid circles with error bars on the right indicate mean values with standard deviation. For each type of GUV membrane composition, the fluorescence intensity was normalized by the mean value of the non-quenched measurement. The dashed lines are guides to the eye indicating the mean

value of non-quenched GUVs, half of the mean value and zero. All measured GUVs had diameters between 20 and 40 µm. The quenching was done with 2.5 mM $Na_2S_2O_4$ final concentration, 5 min incubation followed by 5-fold dilution. The table shows the expected molar fraction of POPG in each leaflet as set by the preparation protocol and the one estimated from the fluorescence intensity after quenching the outer leaflet plus the standard deviation.

2.4. Vesicle stability decreases with increasing membrane charge asymmetry

To assess the effect of membrane asymmetry on GUV stability upon poration, the vesicles were exposed to a single DC pulse (3 kV/cm and 150 µs) and the response was followed with phase contrast optical microscopy. Neutral POPC GUVs typically deformed and the formation of a micrometer-wide pores (macropores) that quickly (~50 ms) reseal could be observed. Subsequently, the pores reseal and the GUVs restore their integrity with preserved contrast, see Figure 5A. When a similar pulse is applied to symmetric vesicles containing high fractions of anionic lipids, additional effects could occur [33]. Some GUVs were apparently restored after macropore closure, but remained in a highly permeable state revealed by the loss of sugar asymmetry within 1 minute, indicating that submicroscopic pores persist after the end of the pulse (leaky vesicles, Figure 5B). Still, another fraction of GUVs collapsed, through the indefinite expansion of a macropore, in a phenomenon called bursting (Figure 5C). To quantify the destabilization brought by the presence of charge asymmetry, we applied single DC pulses to a collection of GUVs and evaluated the fraction of vesicles that exhibited any of these two destabilizing effects (leaky state or bursting), see Figure S1 for more information. The fraction of destabilized vesicles (X_{dest}) was measured for increasing POPG fractions in symmetric and asymmetric GUVs (Figure 5D). The symmetric GUVs were prepared using both electroformation and the inverted emulsion method. Previous studies [33] have shown that electroformed and therefore symmetric GUVs are destabilized only at high POPG fractions > 40 mol%. Surprisingly, here we observe that symmetric GUVs prepared by the inverted emulsion method showed considerable membrane destabilization upon electroporation already for pure POPC membranes (neutral vesicles); compare first data points of black and green traces in Figure 5D. This indicates that GUVs prepared by the inverted emulsion technique are less stable compared to electroformed GUVs with the same membrane composition. Presumably, residual oil in the membrane destabilizes the vesicles upon poration.

We then explored the destabilization fraction X_{dest} for asymmetric GUVs comparing it to that of symmetric GUVs, whereby both were prepared via the inverted emulsion technique. Interestingly, already small charge asymmetries of 5 mol% POPG considerably enhanced the membrane destabilization and were independent on the direction of the asymmetry (aGUVi or aGUVo), Figure 5D. Therefore, we conclude that charge asymmetry indeed plays an important role in membrane destabilization, rendering the membranes more prone to disturbance events and less able to fully reseal even at low molar fractions of charged species.
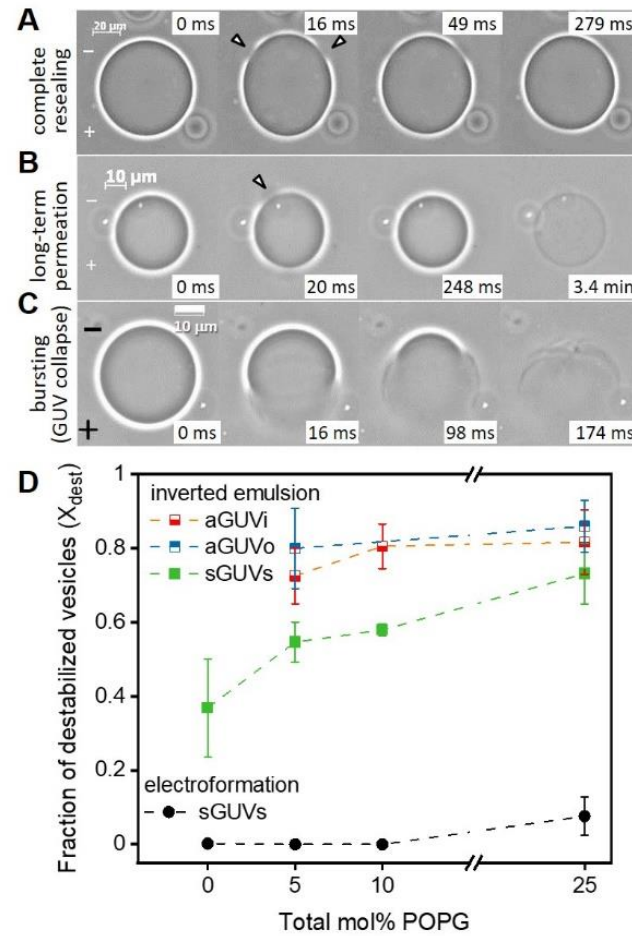
Figure 5: Effect of membrane charge asymmetry on vesicle destabilization upon electroporation. (A-C) Exemplary phase contrast microscopy images showing three possible responses of GUVs to the application of a single DC pulse (3 kV/cm and 150 μs). After the pulse application, micronsized pores (arrowheads) can open and readily reseal restoring GUV integrity (A). Some GUVs that apparently restore their integrity after macropore closure can exhibit high permeability at a later stage revealing the persistence of long-lasting sub-microscopic pores minutes after the end of the pulse (B). In more extreme cases, macropores can open indefinitely leading to vesicle bursting (C). The field polarity is indicated on the first images. (D) Fraction of destabilized vesicles, X_{dest}, (comprising permeating and bursting ones as in panels B and C) for GUVs composed of POPC containing increasing molar fraction of POPG symmetrically and asymmetrically distributed in the membrane leaflets obtained via inverted emulsion method (solid and half-filled squares) and electroformation (solid circles). For GUVs obtained via inverted emulsion approach, average values and standard deviations for measurements on 4 to 6 vesicle preparations per composition are shown (more than 10 vesicles per preparation were monitored). For electroformed GUVs, average values and standard deviations for a number of measurements are shown for 1 vesicle preparation per composition (around 10 vesicles per composition were monitored). Measurements were made in the presence of 0.1 mM EDTA (except for 5 mol% PG sGUVs and aGUVo, prepared via the inverted emulsion protocol.

To explore the origin of vesicle destabilization, we measured the pore edge tension in these membranes. This parameter reflects the work performed to expand the pore boundary by a unit length and is dependent on membrane composition. The edge tension was obtained from the relaxation dynamics of macropore closure, following an approach reported earlier [29] and using an automated image analysis methodology [34]. Since a significant difference in X_{dest} was observed between sGUVs prepared by electroformation or the inverted emulsion protocol, we first compared edge tension values of these two systems. Interestingly, there was no

11

difference in γ when comparing sGUVs of the same composition (pure POPC or POPC with 10 mol% POPG) prepared by both methods (Figure S2). Hence, the observed increased destabilization of vesicles prepared by inverted emulsion was not related to hindering macropore closure in the membrane. We conclude that the specific membrane composition, and in particular, the presence of oil residues, affects the intrinsic membrane response towards destabilization, but the oil molecules are not edge active and thus do not influence the measured edge tension values.

Figure 6 shows the edge tension data measured for aGUVs with increasing molar fraction of POPG asymmetry (green circles and red squares). These results are a compilation of data for aGUVo and aGUVi with and without EDTA, known to remove possible calcium ions as contaminants from the medium [63]. No significant differences were observed for the same fraction of POPG irrespective of the leaflet location or the presence of EDTA (see Figure S3). Data previously measured for sGUVs (grown by electroformation) with the same total fraction of POPG are also shown in Figure 6 for comparison (black data, obtained from Lira et al. [33]). The mean values with standard deviations for all conditions are shown in Table 1. Inverted emulsion GUVs made of pure POPC (0 mol% POPG) have edge tension comparable to literature data [29,33,64,65]. However, aGUVs containing 5, 10 and 17.5 mol% POPG showed a significant edge tension reduction. Comparing vesicles with the same surface charge composition of one of the leaflets, aGUVs containing 25 mol% POPG showed even stronger reduction in the edge tension (~15 pN) compared to sGUVs that expose the same POPG fraction but contain twice higher amount of anionic lipid in total (~23 pN for 50 mol% in total) [33,34], see Table 1.
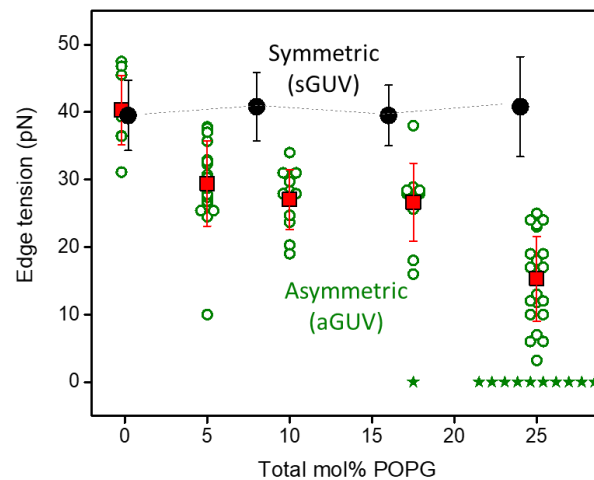

Figure 6: Pore edge tension values of GUVs composed of POPC containing increasing molar fractions of POPG, that were either symmetrically (black solid circles) or asymmetrically distributed (green open circles and red squares). The pore edge tension values for sGUVs are obtained from vesicles produced via electroformation (data published in Lira et al. [33]). The open green circles represent measurements of individual vesicles. Green stars indicate vesicles that burst after the pulse and are indicated as having a value of the edge tension close to 0. The data for pure POPC membranes (0 mol% POPG) are slightly offset in composition for visibility. Since the type of membrane asymmetry (in terms of POPG location in the outer or inner leaflet) did not affect the pore edge tension, the data from aGUVi and aGUVo, with and without EDTA was combined (see also Figure S3). A total of 87 vesicles were measured (10 to 34 vesicles per membrane composition).

Table 1. Edge tension values measured for symmetric (sGUVs) and for asymmetric (aGUVs) of POPC with increasing total mole fraction of POPG. Data indicated with an asterisk are from reference [33].

	Preparation method	Total mol% POPG	Edge tension (pN)
sGUVs	Electroformation	0	40.4 ± 7.9
			$39.5 \pm 5.2*$
		8	$40.8 \pm 5.1*$
		10	40.0 ± 5.1
		16	$39.5 \pm 4.5*$
		24	$40.8 \pm 7.4*$
		50	$23.4 \pm 6.0*$
	Inverted emulsion	0	40.3 ± 5.1
		10	37.9 ± 7.9
aGUVs	Inverted emulsion	0	40.3 ± 5.1
		5	29.4 ± 6.4
		10	27.0 ± 4.4
		17.5	26.6 ± 5.8
		25	15.3 ± 6.3

The edge tension results show that the increase in the molar fraction of POPG results in membranes that are more prone to poration (less energy is needed for pore expansion), and this trend was significantly enhanced when the charges were asymmetrically distributed. A much lower fraction of the charged lipid in the asymmetric membrane compared to the symmetric one is sufficient to cause significant reduction in the edge tension values. When discussing results on sGUVs and aGUVs, we made the comparison based on the total amount of POPG that can either be homogeneously distributed between both monolayers (sGUVs) or almost entirely restricted to one of the monolayers (aGUVs). We also considered the comparison based not on the total POPG amount but on the POPG fraction in the POPG-rich leaflet (in this case, the amount of POPG in the POPG-rich leaflet of asymmetric membranes is almost double the one in the symmetric ones with the same total POPG fraction), because it could be that the POPG-rich leaflet dictates the behavior of the whole bilayer. These analyses for the fraction of destabilized GUVs, X_{dest}, and edge tension are provided in Figure S4. Even when the symmetric membrane has as much POPG as the POPG-rich side of the asymmetric one, aGUVs are still more unstable than sGUVs, both regarding X_{dest} and pore edge tension.

Above we observed that the preparation method had no effect on the edge tension of symmetric membranes. On the other hand, the fraction of destabilized vesicles, X_{dest}, which quantifies the occurrence of leaky membranes and vesicle burst after electroporation, was significantly higher for vesicles prepared by the inverted emulsion protocol, even in symmetric cases. Therefore, we hypothesized that traces of oil used to disperse the lipids from the two different monolayers that are present in the membrane are affecting membrane stability. To confirm that the main source of instability was brought by charge asymmetry, we also generated membrane asymmetry in the GUVs by a very different approach, namely by varying the pH across the membrane.

2.5. Charge asymmetry caused by different pH values across the membrane also destabilizes membranes

The phosphate group of POPG has a pKa around 4 [66]. To generate asymmetry, we prepared sGUVs via electroformation containing 20 mol% POPG at neutral pH and then dispersed the GUVs in low pH solution, so that protonation of POPG in the outer layer generated charge asymmetry across the membrane. Figure 7A shows the fraction of destabilized GUVs after electroporation (X_{dest}) for sGUVs made of POPC with 20 mol% POPG prepared in neutral pH and then dispersed in solutions of different lower pH values down to pH 3. The data show that X_{dest} increases significantly for pH 3, which is below the pKa of the phosphate group, but does not change considerably when the external pH is between 4 and 7 (see blue data points in Figure 7A). As a control, we also prepared GUVs made of pure POPC and of POPC with 50 mol% POPG and measured X_{dest} when the external solution was neutral or at pH 3. As expected, POPC was not destabilized in any pH (black data in Figure 7A), whereas POPC with 50 mol% POPG showed already a significant destabilization at neutral pH, as reported earlier [33], but even stronger when at pH 3 (red data in Figure 7A).
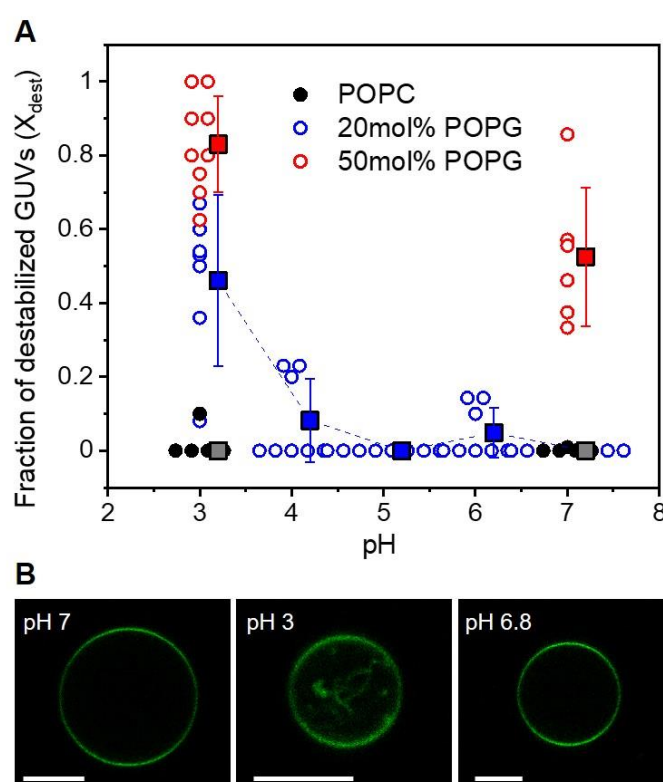

Figure 7: Membrane charge asymmetry generated by different pH across the membrane destabilizes GUVs. (A) Fraction of destabilized vesicles as a function of the external pH of GUVs grown in neutral pH (internal pH 7). Circles show values for each observation chamber and filled squares shown on the right represent the mean values with standard deviation. (B) Representative confocal microscopy images of GUVs of POPC with 20 mol% POPG (0.5 mol% PG-NBD) obtained after dispersing the GUVs of the same sample in pH 7, pH 3 and back to pH 6.8. Scale bars represent 10 μm.

The main concern about this approach is whether the pH asymmetry is indeed maintained during the observation and whether the protonated POPG flips across the membrane, thus obliterating the asymmetry [67]. Since POPG and its analogue counterpart

14

NBD-PG are symmetrically distributed, the quenching assay is of no use here, and in addition, sodium dithionite is much more unstable at acidic pH. Another way to qualitatively confirm the presence of membrane asymmetry is to probe for spontaneous curvature changes expressed in tubulation of GUVs with excess area [53–55]. Since protonated POPG has a smaller area per headgroup than its charged state [68], charge asymmetry will also cause area imbalance giving rise to membrane spontaneous curvature. We noticed that after dispersion of GUVs of POPC with 20 mol% POPG in solutions of pH 3, inward tubes were generated in the GUVs, whereas when no pH asymmetry was present, GUVs were mainly spherical with smooth membrane and free of tubes (see Figure 7B). To show that the asymmetry was maintained after dispersing the GUVs in pH 3, we increased again the pH of the external solution after inner tubes were formed at pH 3. The tubes were suppressed, showing that the area of the external layer was reestablished and brought back to that of the internal one, and no flip-flop of the protonated PG occurred.

In summary, the destabilization effect of charged lipids in asymmetric membranes was already pronounced at low POPG fraction as a result of extremely reduced pore edge tension, whereas anionic sGUVs were only affected at membrane compositions of around 50 mol% POPG. We speculate that one important destabilization factor, in addition to the effect of charged lipids, is a high spontaneous curvature that is caused by the area mismatch between the leaflets of membranes with increased POPG asymmetry.

3. Conclusions

Model membranes such as GUVs can be versatile tools to understand the importance and influence of asymmetry in membranes. To draw the right conclusions, the membranes need to be well characterized. A useful approach to verify membrane asymmetry is the quenching assay, although its application requires precaution. We showed that the stabilization of the dithionite ion and radical is crucial for a successful quenching assay. We identified the optimal conditions for such measurements on GUVs. Our results show that the stability of the quenching agent is improved by preparing low concentrated stock solutions with alkaline pH and short storage durations. To avoid membrane destabilization by the presence of dithionite decomposition products (e.g. hydrogen sulphite and hydrogen sulphate), the dithionite concentration should be adjusted to the minimal quenching concentration and subsequent dilution is required after quenching of the outer leaflet is finished. Despite the multiple reported protocols for quenching assays performed on SUVs, LUVs, GUVs and cells [53,56–58], the needed precaution for the handling of sodium dithionite is often underrated, which makes it difficult for readers to reproduce the experimental protocol. Moreover, different membrane systems can show different membrane permeability of the quenching agent [57,58]. Our work should raise awareness of the demanding character of the used quenching agent and provide a guide to optimize and adjust the quenching conditions for different samples and experimental setups.

Furthermore, we investigated membrane stability upon electroporation as a function of charge asymmetry. The results presented here emphasize the impact of anionic lipids on the stability of model membranes, in which the charge distribution is closer to the reality of the cell membrane. We considered not only the effect of increasing the fraction of charged lipids but also the charge lipid asymmetry existing between the membrane leaflets. The latter was established in two ways – using the inverted emulsion protocol for GUV preparation and as induced by pH asymmetry in the solutions across the membrane. As depicted in the

introduction section, leaflet asymmetry is capable of dictating various cellular functions by modifying the material properties of membranes and although some studies have investigated lipid asymmetry among monolayers, none of them directly addressed the effect of charge asymmetry between them. To our knowledge, this is the first work to show that charge asymmetry plays an important role in cell membrane destabilization and permeability after electroporation. The origin of this destabilization is partially related to changes in membrane composition as reflected in the changes in the edge tension values. This result can be juxtaposed to data showing changes in the bending rigidity of asymmetric *vs* symmetric membranes for the same overall membrane composition [69]. This finding was recently interpreted as potentially arising from differential stress (resulting not from compositional but area difference of the leaflets [70,71]). It remains to be shown whether membrane destabilization as demonstrated here is a result of such differential stress. We expect that our finding for this asymmetry-enhanced destabilization will contribute towards understanding of the arsenal of recovery and pore-resealing mechanisms developed by cells in wound healing processes.

Finally, our results also suggested that the inverted emulsion method for generating asymmetric GUVs adds some instability to the membrane that is still to be investigated but should be considered when studying membrane parameters that can be affected by a possible oil contamination.

4   4. Materials and Methods

4.1   Materials

The lipids 1-palmitoyl-2-oleoyl-sn-glycero-3-phosphocholine (POPC), 1-palmitoyl-2-oleoyl-sn-glycero-3-phospho-(1'-rac-glycerol) (sodium salt) (POPG) and (1-oleoyl-2-{6-[(7-nitro-2-1,3-benzoxadiazol-4-yl)amino]hexanoyl}-sn-glycero-3-[phospho-rac-(1   glycerol)] (ammonium salt)) (NBD-PG) were purchased from Avanti Polar Lipids (Alabaster, AL). Glucose, sucrose, NaCl, EDTA, TrisHCl and sodium dithionite were purchased from Sigma-Aldrich (St. Louis, MO, USA). Lipids and dye were dissolved in chloroform and the stock solutions were stored at -20 °C until use. Alexa647 hydrazide was purchased from Thermo Fischer (Germany). Light mineral oil was purchased from Carl Roth (Karlsruhe, Germany).

4.2   Vesicle preparation via electroformation

For the optimization of the quenching assay, symmetric GUVs were prepared by the electroformation method [72]. Briefly, a lipid mixture (6 µL, 2 mM) dissolved in chloroform was spread on the surfaces of two conductive glasses (coated with indium tin oxide), which, after being dried under a stream of nitrogen, were sandwiched, with a Teflon spacer (2 mm thick) forming a chamber (~2 mL volume). This chamber was filled with sucrose solution (0.2 M) and connected to a function generator. An AC field (1.6 Vpp, 10 Hz) was applied for 30 minutes to accelerate the growth of the GUVs. The vesicles were then harvested and diluted in isotonic sucrose solution. The osmolarity was adjusted with an osmometer (Osmomat 3000, Gonotec GmbH, Germany).

4.3   Vesicle preparation via inverted emulsion technique

The protocol for preparation of GUVs via inverted emulsion technique was adapted from previous work on the method [43,73]. Briefly, the first step consisted in preparing the lipid-in-oil solutions that were used to create the individual monolayers. The lipid mixture for each monolayer was prepared in a glass vial and the chloroform removed under a stream of nitrogen followed by further evaporation in vacuum for 1h. Mineral oil was added to each vial to give an 800 µM and 400 µM solution for the outer and inner leaflets, respectively. Lipids were

16

dissolved in the oil by sonication for 2h. For the preparation of the outer monolayer, 250 µL of glucose (0.18 or 0.58 M, depending on the experiment) were added to a 1.5 mL protein Lo-bind tube (Eppendorf, Germany), followed by the addition of 250 µL of lipid-in-oil for the outer leaflet (800 µM), creating a water-oil column. This column was left to stabilize for 2 hours. The next step, after the 2 hours column incubation, consisted in preparing the emulsion of droplets containing the lipids for the inner monolayer. Lipid in oil for the inner leaflet (150 µL, 400 µM) was placed in a separate 1.5 mL tube, followed by the addition of sucrose (4 µL, 0.2 M or 0.6 M, slightly higher osmolarity than the glucose solution). An emulsion was produced by mechanical agitation, dragging 4 times the tube over a tube rack (Polypropylene, 96 positions). The emulsion was then carefully pipetted and deposited on the top of the water-oil column, followed by centrifugation (130 rcf, 10 minutes). After centrifugation, the residual oil on the top of the glucose solution was thoroughly removed, without extreme perturbation to the interface and the vesicles harvested.

4.4   Imaging of GUVs using optical and confocal microscopy

Different modes of observation were employed. Electroporation experiments for pore edge tension calculation were performed on a Zeiss Axiovert 135 TV (Jena, Germany) phase-contrast inverted microscope equipped with an ultra-fast camera Phantom V2512 (up to 25000 frames per second) or alternatively with an Axio Observer D1 (Jena, Germany) equipped with an sCMOS camera (pco.edge, PCO AG, Kelheim, Germany), for the quantification of GUV response to DC pulse and posterior calculation of the fraction of destabilized vesicles. In both cases, a 20x (NA 0.4) air objective was used. Fluorescence measurements were performed on a Leica confocal SP5 setup (Mannheim, Germany), through a 40x (0.75 NA) air objective. NBD-PG was excited using the 488 nm line of an Argon laser and collected in the 500–600 nm. The Alexa-647 fluorophore was excited using a 638 HeNe laser and the signal was collected between 650-750 nm.

4.5   Python code for measuring membrane fluorescence intensity

The algorithm is provided in the form of Jupyter notebooks, which are files that can be run in a browser. The inputs are ".lif" files, which are the standard file format for Leica confocal microscopes. First, a Gaussian Filter (kernel size of one pixel) was applied to the images to remove noise. To obtain an estimate of the membrane fluorophore concentration, four lines were drawn across the membrane (vertical and horizontal and passing through the GUV center) to generate four intensity profiles. The integrated area below these intensity profiles is proportional to the fluorophore concentration in the membrane and the mean value of these four measurements was used as mean fluorescence intensity. The code can be found in the GitHub depository: https://github.com/fernandaleomil/fluorescenciaguvs

4.6   Membrane asymmetry revealed via leaflet specific fluorophore quench

To assess the asymmetric distribution of POPG in the membrane, the dithionite quenching assay was employed targeting NBD-PG. In the first step, the membrane signal of not quenched GUVs was measured by confocal microscopy imaging at the equatorial plane and image analysis using a custom written python code (see section 4.5). In the next step, the membrane signal of GUVs from a quenched sample was measured and normalized by the mean value obtained on GUVs from the not quenched control sample. At least 20 GUVs were considered for each sample; the scatter in the data results from imaging vesicles of different size (corresponding to different depth in the sample) and inhomogeneity during mixing. The basic procedure of the NBD fluorophore quenching is described in the following (the details for optimizing this protocol are described in section 2.2): freshly prepared sodium dithionite solution (100 mM in 1 M TrisHCl pH 10) was added to a premixed GUV-in-sucrose solution (17.5 µL) and 0.18 M glucose solution (the volume was adjusted to the volume of added

dithionite to obtain a final volume of 100 µL) to final sodium dithionite concentrations of 0.5, 1, 1.5, 2, 2.5 or 10 mM. After a certain incubation time (1, 5, 10 or 15 minutes) the sample was diluted 5-fold with 0.18 M glucose (400 µL), in order to reduce the concentration of sodium dithionite. 100 µL of the sample were used for observation. To optimize the protocol, different sodium dithionite concentrations and incubation times were tested.

4.7   Electroporation experiments

GUVs prepared in sucrose were diluted ~10-fold in glucose solution (at the same solution osmolarity used for GUV preparation) containing the appropriate additive (NaCl and/or EDTA) and placed in an electroporation chamber (Eppendorf, Hamburg, Germany). The chamber consists of two parallel platinum electrodes (92 µm in radius) and 500 µm apart (gap distance). The chamber was connected to a Multiporator (Eppendorf) for DC electric pulse application (3 kV/cm, 150 µs). Experiments to quantify the number of GUVs that underwent bursting or contrast loss (relative to all vesicles in the field, Figure S1) after the DC pulse were performed in glucose (0.58 M) and, if not otherwise indicated, without any additive. Image sequences were typically acquired at 1760 px × 2160 px, with acquisition rate of 10 frames per second, for 5 minutes. Pore edge tension experiments were performed on vesicles grown in the presence of NaCl (0.18 M sucrose and 0.5 mM NaCl) and diluted in glucose to induce oblate deformation during the pulse. Image sequences were typically acquired at 512 px × 512 px with acquisition rates between 3000 to 20000 frames per second. Pore dynamics was assessed with the software PoET [34], where for the viscosity of the outer solution (η) we used 1.133×10^{-3} Pa.s.

Supporting Information
Supporting Information is available from the Wiley Online Library or from the author.

Acknowledgements

Author contributions
RD and KAR proposed and supervised the project. All authors designed the experiments, FL and MS performed the experiments and analyzed the data. FL, MS, RD and KR wrote the manuscript. Fernanda Leomil and Mareike Stephan contributed equally to this work.

Funding

Conflict of Interest
None declared.

References
[1]   Lorent, J.H., Levental, K.R., Ganesan, L., Rivera-Longsworth, G., Sezgin, E., Doktorova, M., Lyman, E., and Levental, I. *Nat. Chem. Biol.*, 2020, 16 (6), 644–652.

[2]   Bretscher, M.S. *Nat. New Biol. 1972 23661*, 1972, 236 (61), 11–12.

[3]   Devaux, P.F. *Biochemistry*, 1991, 30 (5), 1163–1173.

[4]   Fadok, V.A., and Henson, P.M. *Curr. Biol.*, 1998, 8 (19), R693–R695.

[5]   Lentz, B.R. *Prog. Lipid Res.*, 2003, 42 (5), 423–438.

[6]   Riedl, S., Rinner, B., Asslaber, M., Schaider, H., Walzer, S., Novak, A., Lohner, K., and Zweytick, D. *Biochim. Biophys. Acta - Biomembr.*, 2011, 1808 (11), 2638–2645.

[7]   Bevers, E.M., and Williamson, P.L. *Physiol. Rev.*, 2016, 96 (2), 605–645.

[8]   Fadok, V.A., Bratton, D.L., Frasch, S.C., Warner, M.L., and Henson, P.M. *Cell Death Differ.*, 1998, 5 (7), 551–562.

[9]   Callahan, M.K., Williamson, P., and Schlegel, R.A. *Cell Death Differ. 2000 77*, 2000, 7 (7), 645–653.

[10]   Daleke, D.L. *J. Biol. Chem.*, 2007, 282 (2), 821–825.

[11]   van Meer, G. *Cold Spring Harb. Perspect. Biol.*, 2011, 3 (5), 1–11.

[12]   Allhusen, J.S., and Conboy, J.C. *Acc. Chem. Res.*, 2017, 50 (1), 58–65.

[13]   Doktorova, M., Symons, J.L., and Leventhal, I. *Nat. Chem. Biol.*, 2020, 16 (12), 1321–1330.

[14]   McNeil, P.L., and Steinhardt, R.A. *J. Cell Biol.*, 1997, 137 (1), 1.

[15]   McNeil, P.L., and Steinhardt, R.A. *Annu. Rev. Cell Dev. Biol.*, 2003, 19, 697–731.

[16]   Kinosita, K., Ashikawa, I., Saita, N., Yoshimura, H., Itoh, H., Nagayama, K., and Ikegami, A. *Biophys. J.*, 1988, 53 (6), 1015–1019.

[17]   Kinosita, K., and Tsong, T.Y. *Biochim. Biophys. Acta - Biomembr.*, 1977, 471 (2), 227–242.

[18]   Mir, L.M., Orlowski, S., Belehradek, J., and Paoletti, C. *Eur. J. Cancer Clin. Oncol.*, 1991, 27 (1), 68–72.

[19]   Belehradek, M., Domenge, C., Luboinski, B., Orlowski, S., Belehradek, J., and Mir, L.M. *Cancer*, 1993, 72 (12), 3694–3700.

[20]   Mali, B., Jarm, T., Snoj, M., Sersa, G., and Miklavcic, D. *Eur. J. Surg. Oncol.*, 2013, 39 (1), 4–16.

[21]   Frandsen, S.K., Vissing, M., and Gehl, J. *Cancers (Basel).*, 2020, 12 (2), 290.

[22]   Yarmush, M.L., Golberg, A., Serša, G., Kotnik, T., and Miklavčič, D. *Annu. Rev. Biomed. Eng.*, 2014, 16 (1), 295–320.

[23]   Lambricht, L., Lopes, A., Kos, S., Sersa, G., Préat, V., and Vandermeulen, G. *Expert Opin. Drug Deliv.*, 2016, 13 (2), 295–310.

[24]   Keating, A., and Toneguzzo, F. *Prog. Clin. Biol. Res.*, 1990, 333, 491–8.

[25]   Rols, M.P. *Biochim. Biophys. Acta - Biomembr.*, 2006, 1758 (3), 423–428.

[26]   Dimova, R. and Marques, C. *Giant Vesicle B.*, 2019, *The Giant Vesicle Book*.

[27]   Riske, K.A., and Dimova, R. *Biophys. J.*, 2005, 88 (2), 1143–1155.

[28]   Riske, K.A., and Dimova, R. *Biophys. J.*, 2006, 91 (5), 1778–1786.

[29]   Portet, T., and Dimova, R. *Biophys. J.*, 2010, 99 (10), 3264–3273.

[30]   Sabri, E., Aleksanyan, M., Brosseau, C., and Dimova, R. *Bioelectrochemistry*, 2022, 147, 108222.

[31]   Portet, T., Mauroy, C., Démery, V., Houles, T., Escoffre, J.-M., Dean, D.S., and Rols, M.-P. *J. Membr. Biol.*, 2012, 245 (9), 555–564.

[32]   Riske, K.A., Knorr, R.L., and Dimova, R. *Soft Matter*, 2009, 5 (10), 1983.

[33]   Lira, R.B., Leomil, F.S.C., Melo, R.J., Riske, K.A., and Dimova, R. *Adv. Sci.*, 2021, 8 (11), 2004068.

[34]   Leomil, F.S.C., Zoccoler, M., Dimova, R., and Riske, K.A. *Bioinforma. Adv.*, 2021, 1 (1).

[35]   Aleksanyan, M., Lira, R.B., Steinkühler, J., and Dimova, R. *Biophys. J.*, 2022, 121 (17), 3295–3302.

[36]   Brochard-Wyart, F., de Gennes, P.G., and Sandre, O. *Phys. A Stat. Mech. its Appl.*, 2000,

278 (1–2), 32–51.

[37]   Angelova, M.I., Soléau, S., Méléard, P., Faucon, F., and Bothorel, P. *Trends Colloid Interface Sci. VI*, 1992, 127–131.

[38]   Cheng, H.-T., Megha, and London, E. *J. Biol. Chem.*, 2009, 284 (10), 6079–6092.

[39]   Cheng, H.-T., and London, E. *Biophys. J.*, 2011, 100 (11), 2671–2678.

[40]   Visco, I., Chiantia, S., and Schwille, P. *Langmuir*, 2014, 30 (25), 7475–7484.

[41]   Pautot, S., Frisken, B.J., and Weitz, D.A. *Proc. Natl. Acad. Sci. U. S. A.*, 2003, 100 (19), 10718–10721.

[42]   Pautot, S., Frisken, B.J., and Weitz, D.A. *Langmuir*, 2003, 19 (7), 2870–2879.

[43]   Moga, A., Yandrapalli, N., Dimova, R., and Robinson, T. *ChemBioChem*, 2019, 20 (20), 2674–2682.

[44]   Noireaux, V., and Libchaber, A. *Proc. Natl. Acad. Sci.*, 2004, 101 (51), 17669–17674.

[45]   Yeagle, P.L., Hutton, W.C., and Martin, R.B. *J. Biol. Chem.*, 1976, 251 (7), 2110–2112.

[46]   Franzin, C.M., and Macdonald, P.M. *Biochemistry*, 1997, 36 (9), 2360–2370.

[47]   Traïkia, M., Warschawski, D.E., Lambert, O., Rigaud, J.-L., and Devaux, P.F. *Biophys. J.*, 2002, 83 (3), 1443–1454.

[48]   Marquardt, D., Heberle, F.A., Miti, T., Eicher, B., London, E., Katsaras, J., and Pabst, G. *Langmuir*, 2017, 33 (15), 3731–3741.

[49]   Gerelli, Y., Porcar, L., Lombardi, L., and Fragneto, G. *Langmuir*, 2013, 29 (41), 12762–12769.

[50]   Nguyen, M.H.L., DiPasquale, M., Rickeard, B.W., Doktorova, M., Heberle, F.A., Scott, H.L., Barrera, F.N., Taylor, G., Collier, C.P., Stanley, C.B., Katsaras, J., and Marquardt, D. *Langmuir*, 2019, 35 (36), 11735–11744.

[51]   Karamdad, K., Law, R. V., Seddon, J.M., Brooks, N.J., and Ces, O. *Chem. Commun.*, 2016, 52 (30), 5277–5280.

[52]   Lipowsky, R. *Faraday Discuss.*, 2013, 161, 305–331.

[53]   Steinkühler, J., De Tillieux, P., Knorr, R.L., Lipowsky, R., and Dimova, R. *Sci. Rep.*, 2018, 8 (1), 1–9.

[54]   Dasgupta, R., Miettinen, M.S., Fricke, N., Lipowsky, R., and Dimova, R. *Proc. Natl. Acad. Sci.*, 2018, 115 (22), 5756–5761.

[55]   Karimi, M., Steinkühler, J., Roy, D., Dasgupta, R., Lipowsky, R., and Dimova, R. *Nano Lett.*, 2018, 18 (12), 7816–7821.

[56]   McIntyre, J.C., and Sleight, R.G. *Biochemistry*, 1991, 30 (51), 11819–11827.

[57]   Pomorski, T., Herrmann, A., Zachowski, A., Devaux, P.F., and Müllery, P. *Mol. Membr. Biol.*, 1994, 11 (1), 39–44.

[58]   Angeletti, C., and Nichols, J.W. *Biochemistry*, 1998, 37 (43), 15114–15119.

[59]   Enoki, T.A., and Feigenson, G.W. *Biophys. J.*, 2019, 117 (6), 1037–1050.

[60]   Lem, W.J., and Wayman, M. *Can. J. Chem.*, 1970, 48 (5), 776–781.

[61]   Vegunta, V.L. 2016, (June), 272.

[62]   Burlamacchi, L., Guarini, G., and Tiezzi, E. *Trans. Faraday Soc.*, 1969, 65, 496–502.

[63]   Riske, K.A., Döbereiner, H.-G., and Lamy-Freund, M.T. *J. Phys. Chem. B*, 2003, 107 (22), 5391–5392.

[64]   Mattei, B., Lira, R.B., Perez, K.R., and Riske, K.A. *Chem. Phys. Lipids*, 2017, 202, 28–37.

[65]   Casadei, B.R., Dimova, R., and Riske, K.A. *Biophys. J.*, 2018, 114 (3), 94a.

[66]   Watts, A., Harlos, K., Maschke, W., and Marsh, D. *Biochim. Biophys. Acta - Biomembr.*, 1978, 510 (1), 63–74.

[67]   Khalifat, N., Rahimi, M., Bitbol, A.-F., Seigneuret, M., Fournier, J.-B., Puff, N., Arroyo, M., and Angelova, M.I. *Biophys. J.*, 2014, 107 (4), 879–890.

[68]   Khalifat, N., Puff, N., Bonneau, S., Fournier, J.-B., and Angelova, M.I. *Biophys. J.*,

2008, 95 (10), 4924–4933.

[69]   Elani, Y., Purushothaman, S., Booth, P.J., Seddon, J.M., Brooks, N.J., Law, R. V., and Ces, O. *Chem. Commun.*, 2015, 51 (32), 6976–6979.

[70]   Hossein, A., and Deserno, M. *Biophys. J.*, 2020, 118 (3), 624–642.

[71]   Lyman, E., and Sodt, A.J. *Biophys. J.*, 2020, 118 (3), 535–537.

[72]   Angelova, M.I., and Dimitrov, D.S. *Faraday Discuss. Chem. Soc.*, 1986, 81 (0), 303.

[73]   Elani, Y., Purushothaman, S., Booth, P.J., Seddon, J.M., Brooks, N.J., Law, R. V., and Ces, O. *Chem. Commun.*, 2015, 51 (32), 6976–6979.